SIAM J. APPL. MATH.
Vol. 75, No. 2, pp. 652–678

STOCHASTIC ACTIVE-TRANSPORT MODEL OF CELL POLARIZATION*

PAUL C. BRESSLOFF† AND BIN XU†

Abstract. We present a stochastic model of active vesicular transport and its role in cell polarization, which takes into account positive feedback between membrane-bound signaling molecules and cytoskeletal filaments. In particular, we consider the cytoplasmic transport of vesicles on a two-dimensional cytoskeletal network, in which a vesicle containing signaling molecules can randomly switch between a diffusing state and a state of directed motion along a filament. Using a quasi-steady-state analysis, we show how the resulting stochastic hybrid system can be reduced to an advection-diffusion equation with anisotropic and space-dependent diffusivity. This equation couples to a reaction-diffusion equation for the membrane-bound transport of signaling molecules. We use linear stability analysis to derive conditions for the growth of a precursor pattern for cell polarization, and we show that the geometry of the cytoskeletal filaments plays a crucial role in determining whether the cell is capable of spontaneous cell polarization or only polarizes in response to an external chemical gradient. As previously found in a simpler deterministic model with uniform and isotropic diffusion, the former occurs if filaments are nucleated at sites on the cell membrane (cortical actin), whereas the latter applies if the filaments nucleate from organizing sites within the cytoplasm (microtubule asters). This is consistent with experimental data on cell polarization in two distinct biological systems, namely, budding yeast and neuronal growth cones. Our more biophysically detailed model of motor transport allows us to determine how the conditions for spontaneous cell polarization depend on motor parameters such as mean speed and the rate of unbinding from filament tracks.

Key words. cell polarization, stochastic hybrid systems, molecular motors, cytoskeleton, self-organization

AMS subject classification. 92C20

DOI. 10.1137/140990358

1. Introduction.

Many cellular processes depend critically on the establishment and maintenance of polarized distributions of signaling proteins on the plasma membrane. These include cell motility, neurite growth and differentiation, epithileal morphogenesis, embryogenesis, and stem cell differentiation. In many cases, cell polarity can occur spontaneously, in the absence of preexisting spatial cues. One of the most studied model systems of cell polarization is the budding yeast *Saccharomyces cerevisiae* [39, 20]. A yeast cell in the G1 phase of its life cycle is spherical and grows isotropically. It then undergoes one of two fates: either it enters the mitotic phase of the life cycle and grows a bud, or it forms a mating projection (shmoo) toward a cell of the opposite mating type. Both processes involve some form of symmetry breaking mechanism that switches the cell from isotropic growth to growth along a polarized axis; see Figure 1. Under physiological conditions, yeast cells polarize toward an environmental spatial asymmetry. This could be a pheromone gradient in the case of mating or a bud scar deposited on the cell surface from a previous division cycle. However, yeast cells can also undergo spontaneous cell polarization in a random orientation when external asymmetries are removed. For example, in the

*Received by the editors October 7, 2014; accepted for publication (in revised form) February 2, 2015; published electronically April 2, 2015.
http://www.siam.org/journals/siap/75-2/99035.html
†Department of Mathematics, University of Utah, Salt Lake City, UT 84112 (bressloff@math.utah.edu, xu@math.utah.edu). The first author's work was supported by the National Science Foundation (DMS-1120327).

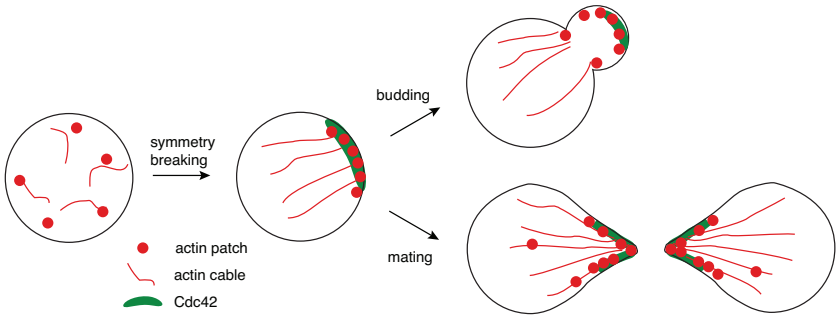

FIG. 1. *Symmetry breaking processes in the life cycle of budding yeast. See text for details. Redrawn from* [39].

case of budding, induced cell mutations can eliminate the recognition of bud scars. Moreover, shmoo formation can occur in the presence of a uniform pheromone concentration. The observation that cells can break symmetry spontaneously suggests that polarization is a consequence of internal biochemical states.

Experimental studies in yeast have shown that cell polarization involves a positive feedback mechanism that enables signaling molecules already localized on the plasma membrane to recruit more signaling molecules from the cytoplasm, resulting in a polarized distribution of surface molecules. The particular signaling molecule in budding yeast is the Rho GTPase Cdc42. As with other Rho GTPases, Cdc42 targets downstream affectors of the actin cytoskeleton [31]. There are two main types of actin structure involved in the polarized growth of yeast cells: cables and patches. Actin patches consist of networks of branched actin filaments nucleated by the Arp2/3 complex at the plasma membrane, whereas actin cables consist of long, unbranched bundles of actin filaments. Myosin motors travel along the cables unidirectionally toward the actin barbed ends at the plasma membrane, transporting intracellular cargo such as vesicles, mRNA, and organelles. The patches act to recycle membrane bound structures to the cytoplasm via endocytosis. During cell polarization, Cdc42-GTP positively regulates the nucleation of both types of actin structure, resulting in a polarized actin network, in which actin patches are concentrated near the site of asymmetric growth and cables are oriented toward the direction of growth. There are at least two independent but coordinated positive feedback mechanisms that can establish cell polarity [42]. One involves the reinforcement of spatial asymmetries by the directed transport of Cdc42 along the actin cytoskeleton to specific locations on the plasma membrane [27, 25], whereas the other involves an actin-independent pathway, in which Bem1, an adaptor protein with multiple binding sites, forms a complex with Cdc42 that enables recruitment of more Cdc42 to the plasma membrane. In the latter case, intrinsic noise plays an essential role in allowing positive feedback alone to account for spontaneous cell polarization [1, 19, 28]. An alternative possibility is that positive feedback is coupled with activity-dependent inhibition [18], resulting in a reaction-diffusion system that exhibits Turing pattern formation [14, 29] or bistability [38, 30, 12].

Probably the most striking example of a polarized cell is the neuron, due to its compartmentalization into a thin, long axon and several shorter, tapered dendrites. Experimental studies of neuronal polarization have mainly been performed on dissociated, embryonic cortical and hippocampal neurons or on postnatal cerebellar granule neurons. Such studies have identified three basic stages of polarization [2, 31]; see

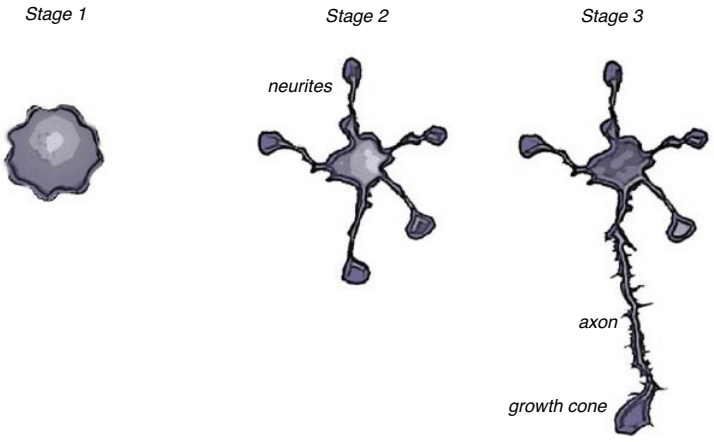

FIG. 2. *Stages of neuronal polarization. A neuron attaches to the substrate as a round sphere surrounded by actin-rich lamellipodia and filopodia (stage* 1*). Growth cones formation by the consolidation of lamellipodia leads to the establishment of several neurites (stage* 2*). One neurite starts to elongate rapidly and forms the axon (stage* 3*).*

Figure 2. Cultured neurons initially attach to their substrate as round spheres surrounded by actin-rich structures including lamellipodia and filopodia (stage 1). Lamellipodia then coalesce to form *growth cones*, followed by the establishment of several short processes, called *neurites* (stage 2). Eventually one of the neurites starts to grow more rapidly to become the axon (stage 3), while the other neurites remain short and develop into dendrites at later stages of maturation. The growth cone at the mobile tip of an elongating neurite or axon contains microtubules within a central domain (C-domain) and actin filaments within the peripheral domain (P-domain); see Figure 3. The microtubules provide the structural backbone of the shaft and a substrate for intracellular transport to the growth cone. They polymerize with their growing ends pointed toward the leading edge of the growth cone. Actin filaments within the P-domain form filopodia and lamellipodia that shape and direct the motility of the growth cone. In both structures, the actin filaments face with their barbed (growing) ends toward the plasma membrane. Polymerization of actin filaments towards the leading edge causes the extension and protrusion of the growth cone. This creates a force that pushes the actin network and the tightly linked plasma membrane backward (retrograde flow) and hinders the invasion of the microtubules into the P-domain. The retrograde flow is also enhanced by the action of myosin molecular motors, which drag the actin cytoskeleton back toward the C-domain, where actin filaments depolymerize at their pointed ends. If there is a balance between actin polymerization in the P-domain and retrograde flow, then there is no elongation. However, signals from surface adhesion receptors bound to a substrate can suppress the retrograde flow of actin filaments, shifting the balance toward polymerization-driven forward motion that involves both actin filaments and microtubules.

The growth cone of an axon can itself exhibit a form of polarization. During neural development, the growth cone has to respond accurately to extracellular chemical gradients that direct its growth. One such gradient activates *gamma-aminobutyric acid* (GABA) receptors in the plasma membrane, which then redistribute themselves asymmetrically toward the gradient source. Single-particle tracking experiments have shown how this redistribution involves interactions between the GABA receptors and

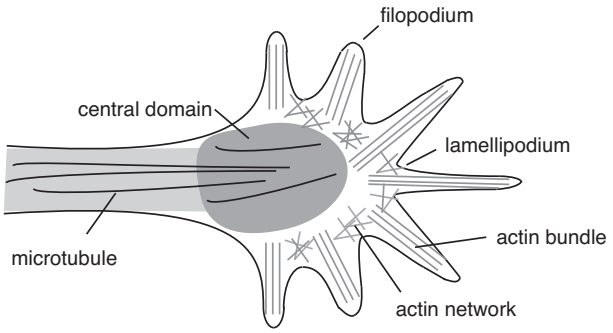

FIG. 3. *Schematic diagram of growth cone showing cytoskeletal structures.*

microtubules in the growth cone, which results in a reorientation of the microtubules toward the gradient source and subsequent steering of the growth cone [4]. Another crucial component is the redistribution of the sites of endocytosis and exocytosis for vesicles carrying lipid proteins to and from the membrane of the growth cone [41]. Interestingly, in contrast to the interactions between Cdc42 and actin in budding yeast, one does not observe spontaneous polarization of the growth cone in the absence of an external spatial cue.

A recent modeling study by Hawkins et al. [15] has demonstrated that the geometry of the organization of cytoskeletal filaments plays a crucial role in determining whether the cell is capable of spontaneous cell polarization or only polarizes in response to an external chemical gradient [15]. More specifically, the authors showed that the former holds if filaments are nucleated at sites on the cell membrane, whereas the latter applies if the filaments nucleate from organizing sites within the cytoplasm (microtubule asters). The model thus captures differences in experimental studies of cell polarization in budding yeast [27, 40] and neuron growth cones [4]. However, the model involves two major simplifying assumptions: (i) the cytoplasmic signaling molecules are treated as free particles rather than bound to vesicles; (ii) the transport of molecules in the cytoplasm is represented in terms of an advection-diffusion process with isotropic, homogeneous diffusion. As highlighted by Layton et al. [25, 37], one potential problem with assumption (i) is that vesicular transport makes cell polarization more difficult to sustain, since fusion of vesicles leads to the release of membrane lipids as well as signaling molecules. This suggests that either there is some active mechanism for increasing the concentration of signaling molecules in the membrane following vesicle fusion, or some other factor is transported by vesicles that maintains cell polarization. Interestingly, experimental evidence for the former mechanism has recently been obtained by establishing that vesicles deliver Cdc42 to sites of polarized growth in yeast [9]. In this paper, we relax both assumptions (i) and (ii) and show that a more biophysically realistic model of active vesicular transport in the cytoplasm leads to an advection-diffusion equation with anisotropic and space-dependent diffusion. Our starting point is a stochastic model of active transport on a two-dimensional cytoskeletal network, in which a vesicle containing signaling molecules can randomly switch between a diffusing state and a state of directed motion along a cytoskeletal filament. Using a quasi-steady-state (QSS) analysis [5, 6], we show how the resulting stochastic hybrid system can be reduced to an advection-diffusion process for the concentration of vesicles in the cytoplasm. We thus derive an explicit expression for the anisotropic diffusion tensor and show how it depends on cytoskeletal geometry.

We then use linear stability analysis to derive conditions for the growth of a precursor pattern for cell polarization and thus demonstrate that our more realistic model of active transport supports spontaneous polarization in the case of nucleation at the cell membrane but not from asters. The effects of spatially varying/anisotropic diffusion and the dependence on various biophysical parameters of the stochastic model are also highlighted. Finally, note that although we do take into account the vesicular nature of active transport (assumption (i)), we do not address the particular issue of lipid transport. However, our more realistic model provides a framework for exploring this issue in future work.

2. The model.

2.1. Deterministic model. We begin by describing the deterministic model of Hawkins et al. [15]. For simplicity, the cell is taken to be two-dimensional and curvature effects are ignored; see Figure 4. The cytoplasm is represented by the semi-infinite domain $(x,z), x \in [-L/2, L/2], z > 0$, with L the circumference of the cell and $z = 0$ the cell membrane. (Boundary conditions at the edges $x = \pm L/2$ are ignored, since the analysis is carried out in the limit $L \to \infty$.) Let $u(x,t)$ denote the concentration of signaling molecules in the membrane and let $c(x,z,t)$ denote the corresponding concentration in the cytoplasm. Hawkins et al. [15] consider a deterministic reaction-diffusion model of the form

$$\frac{\partial u(x,t)}{\partial t} = D_m \frac{\partial^2 u(x,t)}{\partial x^2} + k_{\rm on} c(x,0,t) - k_{\rm off} u(x,t), \tag{2.1a}$$

$$\frac{\partial c(x,z,t)}{\partial t} = D\nabla^2 c(x,z,t) - \mathbf{v}\cdot\nabla c(x,z,t). \tag{2.1b}$$

The first equation represents diffusion of signaling molecules within the membrane together with transfer between the membrane and cytoplasm, where $k_{\rm on}$ and $k_{\rm off}$ are the binding and unbinding rates. The second equation is an advection-diffusion equation that describes the hybrid transport dynamics of molecules in the cytoplasm, which randomly switch between diffusive motion and ballistic motion along the filaments.

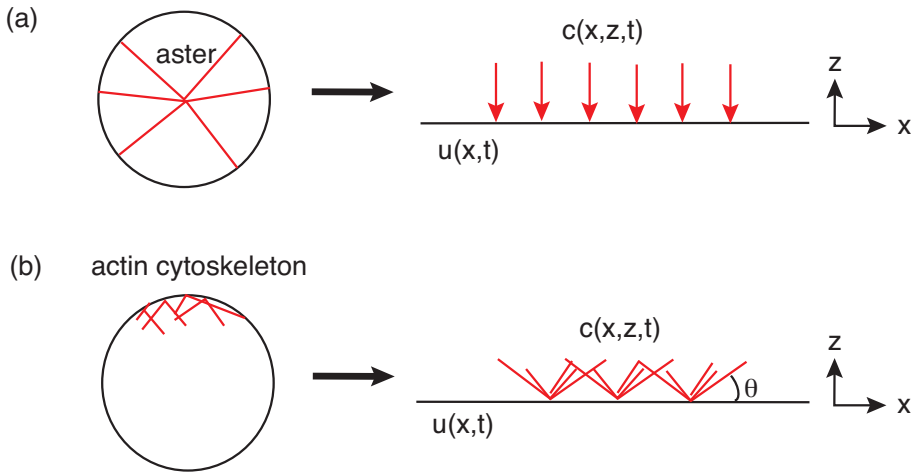

FIG. 4. *Schematic illustration of filament geometry in model of Hawkins et al.* [15]. (a) *Case* (i)*: Nucleation at the cell center.* (b) *Case* (ii)*: Nucleation at the cell membrane.*

In [15] it is assumed that the switching rates are sufficiently high so that the underlying stochastic process can be reduced to the given advection-diffusion process with isotropic diffusion—we will carry out this reduction explicitly in section 2.2 and show that there are additional terms reflecting space-dependent and anisotropic diffusion. The above equations are supplemented by the conservation equation

$$M = \int_{-L/2}^{L/2} u(x,t)dx + \int_{-L/2}^{L/2}\int_0^{\infty} c(x,z,t)dz \tag{2.2}$$

with M the total number of signaling molecules. Since the concentration profile decays exponentially in the z direction, the range of z is taken to be the half-line. Finally, there is conservation of flux at the membrane:

$$k_{\rm on}c(x,0,t) - k_{\rm off}u(x,t) = D\left.\frac{\partial c(x,z,t)}{\partial z}\right|_{z=0} - v_z(x,0,t)c(x,0,t). \tag{2.3}$$

The velocity field $\mathbf{v}(x,z,t)$ depends on the geometry of the filaments, which is itself determined by the concentration of signaling molecules on the membrane. Hawkins et al. [15] distinguish between two cases (see Figure 4):

(i) Filaments that grow from a nucleating center in the cytoplasm (microtubule aster) are approximately perpendicular to the membrane surface. Assuming that the speed of active transport at (x,z) is proportional to the local density of parallel filaments, and that the latter is proportional to the concentration of surface signaling molecules $u(x,t)$, we have

$$\mathbf{v}(x,z,t) = -\kappa_0 u(x,t)\mathbf{e}_z, \tag{2.4}$$

where κ_0 is a constant that specifies the coupling between the signaling molecules and filaments. This type of geometry holds for the distribution of microtubules in neuron growth cones (see Figure 3), where GABA receptors appear to associate with and regulate the growing microtubule ends in the presence of an external chemical gradient [4].

(ii) Filaments that nucleate from sites on the membrane can be approximated by a superposition of asters. Assuming that the velocity field at $\mathbf{r} = (x,z)$ is determined by the local density of filaments, and this decreases with distance from each nucleation site $\mathbf{r}' = (x,0)$, then

$$\mathbf{v}(\mathbf{r},t) = -\kappa_0 \int_{-L/2}^{L/2} \frac{\mathbf{r}-\mathbf{r}'}{|\mathbf{r}-\mathbf{r}'|^2} u(x',t)dx'. \tag{2.5}$$

This geometry reflects the organization of the actin cytoskeleton in budding yeast, as illustrated in Figure 1.

2.2. Stochastic model. One of the assumptions of the Hawkins et al. model [15] is that the stochastic switching between motor-driven transport and diffusion is sufficiently fast that it can be approximated by an advection diffusion process with uniform, isotropic diffusion. However, as we have demonstrated elsewhere, when carrying out the reduction of a stochastic hybrid transport process on a two-dimensional cytoskeletal network, the resulting diffusion process is typically nonuniform and anisotropic [5, 6]; see also [3]. Here we will show that a nontrivial diffusion process occurs for the particular geometries presented in Figure 4. However, in order

to construct a stochastic version of the Hawkins et al. model, we first have to consider active transport processes in a little more detail [8].

The main types of active intracellular transport involve the molecular motors *kinesin* and *dynein* carrying resources along microtubular filament tracks and *myosin V* motors transporting cargo along actin filaments. Microtubules and actin filaments are polarized polymers with biophysically distinct (+) and (−) ends, and this polarity determines the preferred direction in which an individual molecular motor moves. For example, kinesin moves toward the (+) end, whereas dynein moves toward the (−) end of a microtubule. Each motor protein undergoes a sequence of conformational changes after reacting with one or more adenosine triphosphate (ATP) molecules, causing it to step forward along a filament in its preferred direction. Thus, ATP provides the energy necessary for the molecular motor to do work in the form of pulling its cargo along a filament in a biased direction. The movement of molecular motors occurs over several length and time scales [21, 22, 26, 23, 6]. In the case of a single motor there are at least three levels of modeling:

(a) the mechanico-chemical energy transduction process that generates a single step of the motor;
(b) the effective biased random walk along a filament during a single run;
(c) the alternating periods of directed motion along the filament and diffusive or stationary motion when the motor is unbound from the filament.

We will consider level (c) by treating a motor/cargo complex as a particle that randomly switches between a free diffusion state and a ballistic motion state with velocity $\mathbf{V}(\theta)$, $\theta \in [0, \pi]$, where the direction $\arg[\mathbf{V}] = \theta$ is determined by the orientation θ of the cytoskeletal filament at (x, z) to which the complex is bound. Following Hawkins et al. [15], we take $x \in [-L/2, L/2]$ and $z \in \mathbb{R}^+$. The orientation θ is defined as the angle subtended at the cell boundary $z = 0$ (see Figure 4), and we assume that a particle moves toward the plus end of the filament (toward the boundary) with a constant speed v_0. Thus

$$\mathbf{V}(\theta) = -v_0 \cos\theta \mathbf{e}_x - v_0 \sin\theta \mathbf{e}_z. \tag{2.6}$$

The stochastic transport process is illustrated in Figure 5 in the case of parallel filaments with $\theta = \pi/2$ and $\mathbf{V} = -v_0\mathbf{e}_z$. At a sufficiently small spatial scale, the filaments are discrete objects and one would need to specify the spatial location of each filament. We will consider a simplified continuum model under the "homogenization" assumption that the cytoskeletal network is sufficiently dense and ordered. Thus at each point (x, z), there is a density $\rho(x, z, \theta)$ of filaments with the given orientation θ—the probability of binding to any one of these filaments will then be proportional to $\rho(x, z, \theta)$. Ultimately we will take ρ to depend on the concentration of signaling molecules on the membrane surface, so that ρ becomes time-dependent. For the moment, however, we will treat ρ as time-independent.

Let $p_0(x, z, t)$ denote the probability density that the particle is at position (x, z) at time t and is in the diffusive state. Similarly, let $p(x, z, \theta, t)$ be the corresponding probability that it is bound to a microtubule and moving with velocity $\mathbf{V}(\theta)$. Transitions between the diffusing state and the ballistic state are governed by a discrete Markov process. The transition rate β from a ballistic state with velocity $\mathbf{V}(\theta)$ to the diffusive state is taken to be constant, whereas the reverse transition rate is taken to depend on the local density of filaments, $\alpha\rho(x, z, \theta)$. We then have the following Chapman–Kolmogorov (CK) equations describing the evolution of the probability

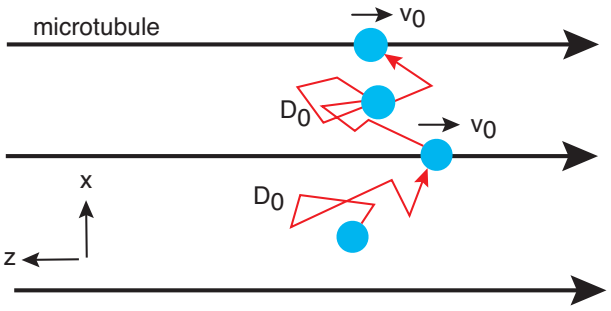

FIG. 5. *Two-dimensional hybrid active transport model, in which vesicles containing polarization signaling molecules are bound to molecular motors that randomly bind to and unbind from filament tracks. When bound, the motor/cargo complex moves ballistically along the given track at a constant velocity v_0, whereas the unbound complex diffuses with a diffusivity D_0. For the sake of illustration, we show parallel tracks.*

densities for $t > 0$:

$$\frac{\partial p(\mathbf{r},\theta,t)}{\partial t} = -\mathbf{V}(\theta)\cdot\nabla p(\mathbf{r},\theta,t) - \frac{\beta}{\epsilon}p(\mathbf{r},\theta,t) + \frac{\alpha\rho(\mathbf{r},\theta)}{\epsilon}p_0(\mathbf{r},t), \tag{2.7a}$$

$$\frac{\partial p_0(\mathbf{r},t)}{\partial t} = \epsilon D_0\nabla^2 p_0(\mathbf{r},t) + \frac{\beta}{\epsilon}\int_0^\pi p(\mathbf{r},\theta,t)d\theta - \frac{\alpha\overline{\rho}(\mathbf{r})}{\epsilon}p_0(\mathbf{r},t), \tag{2.7b}$$

with $\mathbf{r} = (x,z)$ and

$$\overline{\rho}(\mathbf{r}) = \int_0^\pi \rho(\mathbf{r},\theta)d\theta.$$

We have introduced a small dimensionless parameter ϵ, $0 < \epsilon \ll 1$, in order to incorporate the assumption that the switching rates are very fast and diffusion is slow compared to typical motor velocities (on the length scale of a cell). That is, specifying space and time measurements in units of L and L/v_0, we take $\alpha L/v_0 = O(1)$, $\beta L/v_0 = O(1)$, and $D_0/Lv_0 = O(1)$. Note that in the limit $\epsilon \to 0$, the total probability density at each point $\mathbf{r}$ is conserved, that is,

$$\int_0^\pi p(\mathbf{r},\theta,t)d\theta + p_0(\mathbf{r},t) = c(\mathbf{r},t), \qquad \int c(\mathbf{r},t)d\mathbf{r} = 1,$$

where $c(\mathbf{r})$ is determined by the initial conditions. It follows that the system rapidly converges to steady-state distributions

$$(p(\mathbf{r},\theta,t), p_0(\mathbf{r},t)) \to c(\mathbf{r})(p^*(\mathbf{r},\theta), p_0^*(\mathbf{r}))$$

with

$$p_0^*(\mathbf{r}) = \frac{\beta}{\alpha\overline{\rho}(\mathbf{r})+\beta}, \quad p^*(\mathbf{r},\theta) = \frac{\alpha\rho(\mathbf{r},\theta)}{\alpha\overline{\rho}(\mathbf{r})+\beta}. \tag{2.8}$$

Since equations (2.7) are defined in the semi-infinite rectangular domain $x \in [-L/2, L/2], z \in \mathbb{R}^+$, it is necessary to specify boundary conditions along the edges $x = \pm L/2$ and along the cell membrane at $z = 0$. First, we impose periodic boundary conditions with respect to x so that $p(-L/2,z,\theta,t) = p(L/2,z,\theta,t)$ and

$p_0(-L/2,z,t) = p_0(L/2,z,t)$. However, it will be convenient to take the limit $L \to \infty$ when modeling the distribution of microtubules generated by nucleation from the cell membrane, which is reasonable given the exponential decay of the concentrations with respect to z (see below). Second, we impose a no-flux condition along $z = 0$, which requires constructing a probabilistic version of the flux conservation equation (2.3) in order to take into account binding and unbinding of vesicles to the cell membrane. Suppose that if a motor-bound vesicle is in the diffusive state and at the membrane ($z = 0$), then the vesicle can transition to a membrane-bound state and immediately release its contents by fusing with the membrane (exocytosis). Furthermore, we assume that new vesicles form on the membrane and are subsequently released back into the cytoplasm (endocytosis) at a rate that depends on the local density $u(x,t)$ of signaling molecules within the membrane. This is motivated by the observation in yeast that the density of actin patches varies with the membrane density of Cdc42. We then have the following equation for conservation of vesicular flux at the boundary $z = 0$:

$$\epsilon\, D_0 \frac{\partial p_0(x,z,t)}{\partial z}\bigg|_{z=0} + v_0 \int_0^\pi \sin(\theta) p(x,0,\theta,t)\,d\theta = \overline{k}_{\rm on} p_0(x,0,t) - \overline{k}_{\rm off} u(x,t), \tag{2.9}$$

where $\overline{k}_{\rm on}$ and $\overline{k}_{\rm off}$ are the rates of exocytosis and endocytosis, respectively. (Note that $\overline{k}_{\rm on}$ has units of speed as p_0 is density per unit area.) For simplicity, we neglect any time delays associated with the fusion and budding of membrane-bound vesicles. We also assume that there is a dynamic equilibrium of vesicular transport so that the total number of vesicles $M_{\rm ves}$ is fixed:

$$1 = \int_{-L/2}^{L/2} \int_0^\infty \left[\int_0^\pi p(x,z,\theta,t)\,d\theta + p_0(x,z,t) \right] dz\, dx. \tag{2.10}$$

Assuming that each vesicle contains $n_{\rm ves}$ signaling molecules and that protein degradation can be ignored, the total number of signaling molecules M satisfies the conservation equation

$$M = \int_{-L/2}^{L/2} u(x,t)dx + n_{\rm ves} M_{\rm ves} = \text{constant}. \tag{2.11}$$

Finally, the concentration $u(x,t)$ of signaling molecules in the membrane evolves according to

$$\frac{\partial u(x,t)}{\partial t} = \epsilon D_m \frac{\partial^2 u(x,t)}{\partial x^2} + \gamma n_{\rm ves} M_{\rm ves} \left[\overline{k}_{\rm on} p_0(x,0,t) - \overline{k}_{\rm off} u(x,t) \right], \tag{2.12}$$

where γ is a dimensionless conversion factor that determines the change in membrane concentration following endocytosis/exocytosis of a single vesicle. Equation (2.12) is supplemented by the periodic boundary condition $u(-L/2,t) = u(L/2,t)$.

A subtle aspect of constructing the above stochastic model is how to couple the stochastic vesicular dynamics to the distribution $u(x,t)$ of signaling molecules such as Cdc42 within the cell membrane. This raises one of the potential difficulties with the active transport models considered in [27, 15], namely, these models effectively treat transport as a continuous flux of proteins. That is, they don't explicitly take into account the vesicular nature of motor transport. As highlighted by Layton et al. [25, 37], vesicular transport makes cell polarization more difficult to sustain. A simple

argument for this proceeds as follows. First, it is clear that if the concentration of signaling molecules within a vesicle is the same as a local region of membrane, then fusion of the vesicle releases both signaling molecules and additional lipid membrane so the concentration doesn't change, in contrast to a continuous flux of signaling molecules alone. Hence, exocytic vesicles need to have higher concentrations of the signaling molecule than the polarization site in order to enhance the concentration. A dynamic equilibrium of recycling can be maintained only if endocytic vesicles also have an enhanced concentration of signaling molecules. There are various active mechanisms for enhancing the concentration of proteins within vesicles, and although evidence for such processes within the context of cell polarization is currently lacking, it has recently been observed that vesicles do indeed deliver Cdc42 to sites of polarized growth in yeast [9]. We will ignore these issues here and simply assume that each vesicle contains $n_{\rm ves}$ signaling molecules and the membrane concentration increases/decreases by an amount $\gamma n_{\rm ves}$ given a unit flux of vesicles undergoing exo/endocytosis.

Another simplification of our model (and the model of Hawkins et al. [15]) is that the distinction between active/inactive states of Cdc42 is not made in the case of yeast. As highlighted in the introduction, there is also an actin-independent positive feedback mechanism that can establish cell polarity, in which Bem1, an adaptor protein with multiple binding sites, forms a complex with Cdc42 that enables recruitment of more Cdc42 to the plasma membrane. However, it is thought that each mechanism is by itself sufficient to establish cell polarization, suggesting that the presence of two distinct but connected mechanisms leads to greater robustness [42, 39]. In this paper, we focus on the actin-dependent mechanism and show that it alone can support spontaneous polarization.

3. QSS analysis. In order to derive a diffusion approximation of the CK equations (2.7), we will use a QSS approximation. This was first developed from a probabilistic perspective by Papanicolaou [35]; see also [13]. It has subsequently been applied to a wide range of problems in biology [8], including cell movement [34, 16], wave-like behavior in models of slow axonal transport [36, 10, 11], molecular motor-based models of random intermittent search [32, 33], and stochastic neural networks [7]. The QSS approximation is based on the assumption that for $0 < \epsilon \ll 1$, solutions remain close to the steady-state solution. Hence, we set

$$p(\mathbf{r},\theta,t) = c(\mathbf{r},t)p^*(\mathbf{r},\theta) + \epsilon w(\mathbf{r},\theta,t), \tag{3.1a}$$

$$p_0(\mathbf{r},t) = c(\mathbf{r},t)p_0^*(\mathbf{r}) + \epsilon w_0(\mathbf{r},t) \tag{3.1b}$$

with $\mathbf{r} = (x,z)$ and

$$c(\mathbf{r},t) = \int_0^\pi p(\mathbf{r},\theta,t)d\theta + p_0(\mathbf{r},t), \quad \int_0^\pi w(\mathbf{r},\theta,t)d\theta + w_0(\mathbf{r},t) = 0. \tag{3.2}$$

Furthermore, for concreteness, the initial conditions are taken to be

$$c(\mathbf{r},0) = \delta(\mathbf{r}-\mathbf{X}), \quad w(\mathbf{r},\theta,0) = w_0(\mathbf{r},0) = 0,$$

which are equivalent to the following initial conditions for the full probability densities:

$$p(\mathbf{r},\theta,0) = \delta(\mathbf{r}-\mathbf{X})p^*(\mathbf{X},\theta),\ p_0(\mathbf{r},0) = \delta(\mathbf{r}-\mathbf{X})p_0^*(\mathbf{X}).$$

That is, we assume that the system starts on the slow manifold so fast transients can be ignored. One could equally well assume a uniform initial condition for c with respect to position $\mathbf{r}$.

Perturbation and projection methods can now be used to derive a closed equation for the scalar component $c(\mathbf{r},t)$ [5]. First, integrating (2.7a) with respect to θ and adding to (2.7b) yields (to first order in ϵ)

$$\begin{aligned}\frac{\partial c(\mathbf{r},t)}{\partial t} &= \epsilon D_0 \nabla^2 p_0(\mathbf{r},t) - \int_0^\pi \mathbf{V}(\theta)\cdot\nabla p(\mathbf{r},\theta,t)d\theta \\ &= \epsilon D_0\nabla^2[p_0^*(\mathbf{r})c(\mathbf{r},t)] - \int_0^\pi \mathbf{V}(\theta)\cdot\nabla[p^*(\mathbf{r},\theta)c(\mathbf{r},t)]d\theta \\ &\quad - \epsilon\int_0^\pi \mathbf{V}(\theta)\cdot\nabla w(\mathbf{r},\theta,t)d\theta. \end{aligned} \tag{3.3}$$

Next, substituting (3.1a) and (3.1b) into (2.7a) and (2.7b) yields

$$\begin{aligned} p^*(\mathbf{r},\theta)\frac{\partial c(\mathbf{r},t)}{\partial t} + \epsilon\frac{\partial w(\mathbf{r},\theta,t)}{\partial t} &= -\mathbf{V}(\theta)\cdot\nabla\left[p^*(\mathbf{r},\theta)c(\mathbf{r},t)+\epsilon w(\mathbf{r},\theta,t)\right] - \beta w(\mathbf{r},\theta,t) \\ &\quad + \alpha\rho(\mathbf{r},\theta)w_0(\mathbf{r},t) \end{aligned} \tag{3.4}$$

and

$$\begin{aligned} p_0^*(\mathbf{r})\frac{\partial c(\mathbf{r},t)}{\partial t} + \epsilon\frac{\partial w_0(\mathbf{r},t)}{\partial t} &= \epsilon D_0\nabla^2\left(p_0^*(\mathbf{r})c(\mathbf{r},t)+\epsilon w_0(\mathbf{r},t)\right) + \beta\int_0^\pi w(\mathbf{r},\theta,t)d\theta \\ &\quad - \alpha\overline{\rho}(\mathbf{r})w_0(\mathbf{r},t). \end{aligned} \tag{3.5}$$

Now substitute (3.3) into (3.4) and (3.5) and introduce the asymptotic expansion

$$w \sim w^{(0)} + \epsilon w^{(1)} + \cdots$$

Collecting terms to leading order in ϵ and using (3.2) then gives

$$w_0^{(0)}(\mathbf{r},t) \sim \frac{p_0^*(\mathbf{r})}{\alpha\overline{\rho}(\mathbf{r})+\beta}\int_0^\pi \mathbf{V}(\theta)\cdot\nabla(p^*(\mathbf{r},\theta)c(\mathbf{r},t))d\theta \tag{3.6}$$

and

$$\begin{aligned} w^{(0)}(\mathbf{r},\theta,t) &\sim \frac{1}{\beta}\left[1+\frac{\beta}{\alpha\overline{\rho}(\mathbf{r})+\beta}\right]\frac{\alpha\rho(\mathbf{r},\theta)}{\alpha\overline{\rho}(\mathbf{r})+\beta}\int_0^\pi \mathbf{V}(\theta)\cdot\nabla(p^*(\mathbf{r},\theta)c(\mathbf{r},t))d\theta \\ &\quad - \frac{1}{\beta}\mathbf{V}(\theta)\cdot\nabla p^*(\mathbf{r},\theta)c(\mathbf{r},t). \end{aligned} \tag{3.7}$$

Finally, substituting (3.6) and (3.7) into (3.3) yields to $O(\epsilon)$ the Fokker–Planck equation

$$\begin{aligned} \frac{\partial c}{\partial t} &= -\int_0^\pi \mathbf{V}(\theta)\cdot\nabla[p^*(\mathbf{r},\theta)c(\mathbf{r},t)]d\theta + \epsilon D_0\nabla^2[p_0^*(\mathbf{r})c(\mathbf{r},t)] \\ &\quad + \frac{\epsilon}{\beta}\int_0^\pi \mathbf{V}(\theta)\cdot\nabla\left[\mathbf{V}(\theta)\cdot\nabla(p^*(\mathbf{r},\theta)c(\mathbf{r},t))\right] \\ &\quad - \frac{\epsilon}{\beta}\int_0^\pi \mathbf{V}(\theta)\cdot\nabla\left[[1+b(\mathbf{r})]a(\mathbf{r})\frac{\rho(\mathbf{r},\theta)}{\overline{\rho}(\mathbf{r})}\int_0^\pi \mathbf{V}(\theta')\cdot\nabla(p^*(\mathbf{r},\theta')c(\mathbf{r},t))d\theta'\right], \end{aligned} \tag{3.8}$$

where

$$a(\mathbf{r}) = \frac{\alpha\bar{\rho}(\mathbf{r})}{\alpha\bar{\rho}(\mathbf{r})+\beta}, \quad b(\mathbf{r}) = \frac{\beta}{\alpha\bar{\rho}(\mathbf{r})+\beta}. \tag{3.9}$$

Dropping $O(\epsilon)$ corrections to the effective drift velocity, this simplifies to

$$\frac{\partial c}{\partial t} = -\int_0^\pi \mathbf{V}(\theta)\cdot\nabla[p^*(\mathbf{r},\theta)c(\mathbf{r},t)]d\theta + \epsilon\sum_{i,j=x,z} D_{ij}(\mathbf{r})\frac{\partial^2 c(\mathbf{r},t)}{\partial r_i \partial r_j}, \tag{3.10}$$

where

$$D_{ij}(\mathbf{r}) = b(\mathbf{r})D_0\delta_{ij} + Q_{ij}(\mathbf{r}) \tag{3.11}$$

with

$$\begin{aligned} Q_{ij}(\mathbf{r}) = \frac{1}{\beta}\int_0^\pi\int_0^\pi \frac{\rho(\mathbf{r},\theta)}{\overline{\rho}(\mathbf{r})}a(\mathbf{r})V_i(\theta)V_j(\theta') \\ \times\left[\delta(\theta-\theta') - [1+b(\mathbf{r})]a(\mathbf{r})\frac{\rho(\mathbf{r},\theta')}{\overline{\rho}(\mathbf{r})}\right]d\theta d\theta' \geq 0. \end{aligned} \tag{3.12}$$

We now make the simplifying assumption that the density of filaments is sufficiently small so that $\alpha\bar{\rho}(\mathbf{r}) \ll \beta$ for all $\mathbf{r}$, which implies

$$a(\mathbf{r}) \approx \frac{\alpha\bar{\rho}(\mathbf{r})}{\beta} \ll 1, \quad b(\mathbf{r}) = 1 - a(\mathbf{r}), \tag{3.13}$$

This approximation allows us to greatly simplify the analysis without losing the basic structure of the equations and to link up with the analysis of Hawkins et al. [15]. (A biophysical justification of such an approximation would require a more detailed analysis of the interaction between a diffusing motor/cargo complex and a cytoskeletal network. It is motivated by the idea that the unbinding rate from a single filament is independent of other filaments, whereas binding to a filament involves competition with other neighboring filaments. From a mathematical prospective, one would need to take into account the discrete nature of the cytoskeletal network using homogenization theory, for example.) Carrying out a perturbation expansion of (3.10) with respect to $a(\mathbf{r})$ and keeping only leading order terms gives

$$\frac{\partial c}{\partial t} = -\nabla\cdot[\mathbf{v}(\mathbf{r})c(\mathbf{r},t)] + \epsilon\sum_{i,j=x,z} D_{ij}(\mathbf{r})\frac{\partial^2 c(\mathbf{r},t)}{\partial r_i\partial r_j}, \tag{3.14}$$

where

$$\mathbf{v}(\mathbf{r}) = \frac{\alpha}{\beta}\int_0^\pi \mathbf{V}(\theta)\rho(\mathbf{r},\theta)d\theta \tag{3.15}$$

and $D_{ij} = D_0[1-a(\mathbf{r})]\delta_{ij} + Q_{ij}$ with

$$Q_{ij}(\mathbf{r}) = \frac{\alpha}{\beta^2}\int_0^\pi \rho(\mathbf{r},\theta)V_i(\theta)V_j(\theta)d\theta. \tag{3.16}$$

Note that we also ignore $O(\epsilon)$ corrections to the drift term and take the nonuniform diffusion matrix to be outside the second order derivatives.

Finally, it is necessary to determine the boundary condition for $c(\mathbf{r},t)$ by applying the QSS approximation to the flux conservation equation (2.9). In order to relate our QSS approximation to the Hawkins et al. model, we rescale $c(\mathbf{r},t)$ according to

$c(\mathbf{r},t) \to n_{\rm ves}M_{\rm ves}c(\mathbf{r},t)$ so that it can be reinterpreted as the concentration of Cdc42 in the cytosol. Using (3.1a) and keeping only lowest order terms in ϵ then gives

$$\epsilon \sum_j D_{zj}(x,z)\frac{\partial c(x,z,t)}{\partial r_j}\bigg|_{z=0} - v_z(x)c(x,0,t) = k_{\rm on}(x)c(x,0,t) - k_{\rm off}u(x,t) \tag{3.17}$$

with

$$v_z(x) = -\frac{\alpha v_0}{\beta}\int_0^\pi \rho(x,0,\theta)\sin\theta d\theta \tag{3.18}$$

and

$$k_{\rm on}(x) = \gamma \bar{k}_{\rm on}\left[1 - a(x,0)\right], \quad k_{\rm off} = \gamma M_{\rm ves}n_{\rm ves}\overline{k}_{\rm off}. \tag{3.19}$$

Moreover, (2.12) becomes

$$\frac{\partial u(x,t)}{\partial t} = \epsilon D_m \frac{\partial^2 u(x,t)}{\partial x^2} + \left[k_{\rm on}(x)c(x,0,t) - k_{\rm off}u(x,t)\right], \tag{3.20}$$

and the conservation equations (2.10) and (2.11) reduce to

$$M = \int_{-L/2}^{L/2}\int_0^\infty c(x,z,t)dz + \int_{-L/2}^{L/2} u(x,t)dx. \tag{3.21}$$

In the above QSS analysis, we have determined the diffusion coefficients to $O(\epsilon)$ and all other coefficients to $O(1)$. This approximation still holds if we take the density of filaments ρ to depend on the membrane-bound concentration $u(x,t)$ of Cdc42, even though ρ becomes time-dependent, since the evolution of u is much slower than the transition rates between mobile states. Hence, starting from a biophysically detailed stochastic model of motor transport, we have derived an effective reaction-diffusion equation given by (3.14) and (3.20) together with the conservation equations (3.17) and (3.21). Our model is similar in structure to the more phenomenological model of Hawkins et al. [15] (see (2.1), (2.2), and (2.3)), with two significant differences:

(i) The velocity field $v(\mathbf{r})$ in the drift term of (3.14) has a direct biophysical interpretation in the terms of the distribution of polymer filaments and the rates of binding/unbinding of molecular motors. As we show below, this requires modifying the aster velocity field introduced by Hawkins et al. [15].

(ii) The effective diffusion of cytosolic Cdc42, which reflects the stochastic nature of motor transport, is anisotropic. If we set $D_{ij} = D_0\delta_{i,j}$, then (3.14) is identical in form to (2.1) of the Hawkins et al. model.

In the following section we will use our modified reaction-diffusion model to determine conditions for spontaneous pattern formation in the two geometric configurations shown in Figure 4, extending the previous analysis of Hawkins et al. [15]. Recall that in order to derive the deterministic reaction-diffusion model from our stochastic model, we introduced a small parameter ϵ, based on the assumption that transitions between diffusive and motor-driven state are fast relative to diffusion in the cytosol, which is itself faster than membrane-bound diffusion. In our analysis of pattern formation, we reabsorb the factors of ϵ and deal with physical parameters. Finally, following standard treatments of cell polarization, we assume that membrane diffusion is slower than cytoplasmic diffusion by taking $D_m \ll D_0$. However, this inequality could be mitigated by the fact that we are modeling the diffusion of vesicles in the cytoplasm, which tends to be slower than that of single molecules due to molecular crowding.

4. Linear stability analysis and dispersion curves.

4.1. Case (i): Parallel filaments. In the particular example of parallel fibers that are orthogonal to the cell membrane and have a density proportional to $u(x,t)$ (see Figure 4(a)), we have

$$\rho(\mathbf{r},\theta) \to \rho(\mathbf{r},\theta,t) = \kappa u(x,t)\delta(\theta-\pi/2), \tag{4.1}$$

which implies that $\overline{\rho}(\mathbf{r},t) = \kappa u(x,t)$. Substituting into (3.15) shows that this choice of fiber density recovers the velocity distribution (2.4) of Hawkins et al.:

$$\mathbf{v}(\mathbf{r}) = -\frac{\alpha\kappa}{\beta}v_0 u(x,t)\int_0^\pi [\cos\theta\mathbf{e}_x + \sin\theta\mathbf{e}_z]\delta(\theta-\pi/2)d\theta = -\frac{\alpha\kappa}{\beta}v_0 u(x,t)\mathbf{e}_z,$$

which is identical to (2.4) on setting

$$\kappa_0 = \eta v_0, \quad \eta = \frac{\alpha\kappa}{\beta}. \tag{4.2}$$

For the given density, (3.14) and (3.20) then reduce to

$$\frac{\partial c}{\partial t} = \eta v_0 u(x,t)\frac{\partial c(\mathbf{r},t)}{\partial z} + D(x,t)\nabla^2 c(\mathbf{r},t) + Q_{zz}(x,t)\frac{\partial^2 c(\mathbf{r},t)}{\partial z^2} \tag{4.3}$$

and

$$\frac{\partial u(x,t)}{\partial t} = D_m\frac{\partial^2 u(x,t)}{\partial x^2} + \left[k_{\rm on}(x)c(x,0,t) - k_{\rm off}u(x,t)\right]. \tag{4.4}$$

where

(4.5)

$$D(x,t) = D_0[1-\eta u(x,t)], \quad Q_{zz}(x,t) = \frac{\eta v_0^2}{\beta}u(x,t), \quad k_{\rm on}(x) = \gamma\bar{k}_{\rm on}\left[1-\eta u(x,t)\right].$$

Equations (4.3) and (4.4) have an x-independent steady-state solution $c(x,z,t) = c(z)$, $u(x,t) = u^*$ satisfying the pair of equations

$$0 = k_{\rm on}^* c(0) - k_{\rm off}u^*, \quad 0 = D_{zz}^*\frac{d^2c(z)}{dz^2} + \eta v_0 u^*\frac{dc(z)}{dz} \tag{4.6}$$

with

$$D_{zz}^* = D_0[1-\eta u^*] + Q_{zz}^*, \quad Q_{zz}^* = \frac{\eta v_0^2}{\beta}u^*, \quad k_{\rm on}^* = \gamma\bar{k}_{\rm on}\left[1-\eta u^*\right]. \tag{4.7}$$

After imposing a zero flux boundary condition at the membrane surface, we see that

$$u^* = \frac{k_{\rm on}^*}{k_{\rm off}}c(0), \quad c(z) = c(0)\mathrm{e}^{-\xi z}, \quad \xi = v_0\eta u^*/D_{zz}^*. \tag{4.8}$$

Note that the condition $a(\mathbf{r}) \ll 1$ implies that $\xi D_{zz}^* \ll v_0$.

4.1.1. Stability analysis. The stability of the steady-state is determined by substituting

$$u(x,t) = u^* + U(k)\mathrm{e}^{ikx+\lambda t}, \quad c(x,z,t) = c(z) + C(k,z)\mathrm{e}^{ikx+\lambda t}$$

into (4.3) and (4.4) and Taylor expanding to first order in $U(k)$ and $C(k,z)$. The resulting linear equations are

(4.9a)
$$(\lambda + D_m k^2 + k_{\rm off}[1+\eta u^*])U(k) = k^*_{\rm on} C(k,0),$$

(4.9b)
$$(\lambda + D_0^* k^2)C(k,z) = D^*_{zz}\frac{d^2C(k,z)}{dz^2} + \eta v_0 u^* \frac{dC(k,z)}{dz} + \left[\frac{\eta v_0^2}{\beta} - \eta D_0\right]\frac{d^2c(z)}{dz^2}U(k) + \eta v_0 \frac{dc(z)}{dz}U(k)$$

with $D_0^* = D_0(1-\eta u^*)$. On eliminating $U(k)$ and using (4.8), (4.9b) becomes

$$(\lambda + D_0^* k^2)C(k,z) = D^*_{zz}\frac{d^2C(k,z)}{dz^2} + \eta v_0 u^* \frac{dC(k,z)}{dz} + \mathrm{e}^{-\xi z}\frac{F(\xi)}{\lambda + D_m k^2 + [1+\eta u^*]k_{\rm off}}C(k,0)$$

with

$$F(\xi) = k_{\rm off}(\eta u^* \xi)\left(\left[\frac{v_0^2}{\beta} - D_0\right]\xi - v_0\right) = \frac{k_{\rm off} D^*_{zz}\xi^2}{v_0}\left(\left[\frac{v_0^2}{\beta} - D_0\right]\xi - v_0\right).$$

This has a solution of the form

$$C(k,z) = A\mathrm{e}^{-\xi z} + [C(k,0) - A]\mathrm{e}^{-\rho z},$$

where ρ is the positive real root of the equation[1]

$$\rho^2 - \xi\rho - \frac{\lambda}{D^*_{zz}} - \frac{D_0^*}{D^*_{zz}}k^2 = 0,$$

which gives

$$\rho = \frac{1}{2}\left[\xi + \sqrt{\xi^2 + 4(D_0^* k^2 + \lambda)/D^*_{zz}}\right]$$

and

(4.10)
$$A = \frac{1}{(\lambda + D_0^* k^2)}\frac{F(\xi)}{\lambda + D_m k^2 + k_{\rm off}[1+\eta u^*]}C(k,0).$$

[1]For sufficiently negative λ it is possible for ρ to become complex-valued. However, this case does not play a role in the construction of the dispersion relation. It is also physically irrelevant, since it does not represent an instability of the steady-state.

4.1.2. Dispersion relation. In order to derive the dispersion relation $\lambda = \lambda(k)$, we impose the zero-flux condition (3.17), which has the specific form

$$\begin{aligned} &-(D(x,t)+Q_{zz}(x,t))\frac{\partial c(x,0,t)}{\partial z} - \eta v_0 u(x,t)c(x,0,t) \\ &\quad + k_{\rm on}(x)c(x,0,t) - k_{\rm off}u(x,t) = 0. \end{aligned} \tag{4.11}$$

Substituting the linearized solution gives

(4.12)

$$\begin{aligned} &D^*_{zz}\left[(\xi-\rho)A + \rho C(k,0)\right] + \eta\xi\left(\frac{v_0^2}{\beta} - D_0\right)c(0)U(k) - \eta v_0 u^* C(k,0) - \eta v_0 c(0)U(k) \\ &\quad + k^*_{\rm on}C(k,0) - k_{\rm off}(1+\eta u^*)U(k) = 0. \end{aligned}$$

Combining (4.10) and (4.13) and using (4.8) yields the characteristic equation

$$\begin{aligned} 0 \;=\; &\left(\frac{F(\xi)}{k_{\rm off}\xi} - k^*_{\rm on}(1+\eta u^*)\right)\frac{k_{\rm off}}{\lambda + D_m k^2 + k_{\rm off}[1+\eta u^*]} \\ &+ k^*_{\rm on} - D^*_{zz}(\xi-\rho) + \frac{D^*_{zz}(\xi-\rho)}{(\lambda + D_0^* k^2)}\cdot\frac{F(\xi)}{\lambda + D_m k^2 + k_{\rm off}[1+\eta u^*]}, \end{aligned} \tag{4.13}$$

which can be rearranged as

$$\begin{aligned} 0 \;=\; &\left(\frac{F(\xi)}{k_{\rm off}\xi} - (1+\eta u^*)D^*_{zz}(\xi-\rho)\right)\frac{k_{\rm off}}{D^*_{zz}} \\ &+ \left(\frac{k^*_{\rm on}}{D^*_{zz}} - (\xi-\rho)\right)\left[\lambda + D_m k^2\right] + \frac{(\xi-\rho)}{\lambda + D_0^* k^2}F(\xi). \end{aligned} \tag{4.14}$$

Note that the characteristic equation of Hawkins et al. [15] is recovered by taking $v_0\xi/\beta \to 0$ and $\eta u^* \to 0$ (all other terms fixed). Then $D_0^* = D^*_{zz} = D_0$, $k^*_{\rm on} = \bar{k}_{\rm on}$, and $F(\xi) = -D_0\xi^2 k_{\rm off}$ in (4.14):

$$\begin{aligned} 0 = (\lambda + D_0 k^2)&\left[k_{\rm off}(\rho - 2\xi) + \left(\frac{\bar{k}_{\rm on}}{D_0} - (\xi-\rho)\right)\left[\lambda + D_m k^2\right]\right] \\ &- \xi^2 D_0 k_{\rm off}(\xi - \rho). \end{aligned} \tag{4.15}$$

Following Hawkins et al. [15], we express k and ξ in units of R^{-1} and choose the following parameter values:

$$D_0 = 0.1\,\mu m^2\,s^{-1},\; D_m = 0.01\,\mu m^2\,s^{-1},\; R = 10\,\mu m,\; k_{\rm off} = 0.1 s^{-1},\; \bar{k}_{on} = 1\,\mu m s^{-1},$$

with $\gamma = 1$. There is then one free parameter in (4.15), namely, the spatial decay rate ξ. On the other hand, the full dispersion relation (4.14) depends on the additional parameters $\eta u^*, v_0$, and β. Equation (4.8) shows that u^* is proportional to $c(0)$, and the latter is determined by the conservation equation (3.21). Moreover, $\eta = \kappa\alpha/\beta$ is proportional to the strength of coupling κ between the membrane-bound signaling molecules and the distribution of filaments. Equation (4.8) also implies that ξ is related to the other free parameters according to

$$\xi = \frac{v_0\eta u^*}{D_0[1-\eta u^*] + \eta u^*(v_0^2/\beta)}.$$

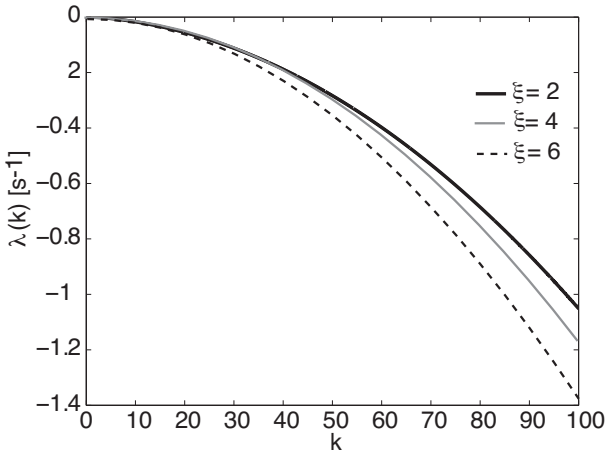

FIG. 6. *Dispersion curves in the case of parallel filaments for various values of ξ. Parameters: $D_0 = 0.1\,\mu m^2\,s^{-1}$, $D_m = 0.01\,\mu m^2\,s^{-1}$, $R = 10\,\mu m$, $k_{\rm off} = 0.1 s^{-1}$, $\bar{k}_{on} = 1\,\mu m s^{-1}$, $v_0 = 1\,\mu m s^{-1}$, $\beta = 1 s^{-1}$. Both ξ and k are in units of R^{-1}*

Recall that we are working in a parameter regime for which ηu^* is small—this then puts constraints on the allowed range of ξ i.e. ξ cannot be too large. However, this is not a major restriction given the parameter regime we are considering. (One could also relax the constraint on ηu^*, although this introduces several additional terms into the dispersion relation and greatly complicates the analysis.) In Figure 6 we show typical dispersion curves $\lambda = \lambda(k)$ in the case of parallel filaments for various values of ξ and $v_0 = 1 \mu m s^{-1}, \beta = 1 s^{-1}$. Consistent with the findings of Hawkins et al. [15], the parallel configuration does not support spontaneous cell polarization.

4.2. Case (ii): Nucleation at the cell membrane. Now suppose that the probability density of a filament of orientation θ at (x, z) depends on the concentration of nucleated asters at location $(x', 0)$ on the membrane such that (see Figure 4(b))

$$\tan(\theta) = \frac{z}{x - x'}.$$

The trigonometric construction is illustrated in Figure 7. Assume that the concentration of asters at $(x', 0)$ is proportional to the density of Cdc42 at that location. The density of filaments from a single aster at $(x', 0)$ will vary as the inverse of the Euclidean distance $|\mathbf{r}| = \sqrt{(x - x')^2 + z^2}$ from the aster. On the other hand, the density of asters contributing to fibers passing through (x, z) and subtending an angle θ will vary as $\sin\theta dx'$ so that

$$\rho(x, z, \theta, t) d\theta = \frac{\kappa}{\pi} \frac{u(x - x', t)}{\sqrt{(x - x')^2 + z^2}} \sin\theta dx'. \tag{4.16}$$

Since

$$\sin\theta = \frac{z}{\sqrt{(x - x')^2 + z^2}},$$

and $dx' = (z/\sin^2\theta) d\theta$, we see that

$$\rho(x, z, \theta, t) = \frac{\kappa}{\pi} u(x - x', t) = \frac{\kappa}{\pi} u(x - z\,\mathrm{cotan}\theta, t). \tag{4.17}$$

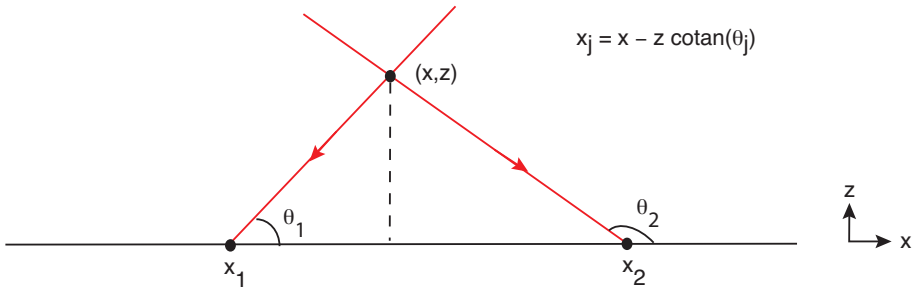

FIG. 7. *Construction of filament density due to nucleation of asters at membrane.*

Note that the range of θ will depend on L. That is, $\theta \in [\theta_-(\mathbf{r}), \theta_+(\mathbf{r})]$ such that

$$\theta_+(\mathbf{r}) = \pi - \tan^{-1}\frac{z}{L/2 - x}, \quad \theta_-(\mathbf{r}) = \tan^{-1}\frac{z}{x + L/2}.$$

Substituting into (3.15) shows that the fiber density (4.17) generates a similar mean velocity distribution (2.5) to Hawkins et al. [15]. That is,

$$\begin{aligned}
\mathbf{v}(\mathbf{r},t) &= -\frac{\alpha\kappa}{\beta\pi} v_0 \int_{\theta_-(\mathbf{r})}^{\theta_+(\mathbf{r})} [\cos\theta \mathbf{e}_x + \sin\theta \mathbf{e}_z] u(x - z\mathrm{cotan}\theta, t) d\theta \\
&= -\frac{\alpha\kappa}{\beta\pi} v_0 \int_{-L/2}^{L/2} \left[\frac{x - x'}{(x-x')^2 + z^2}\mathbf{e}_x + \frac{z}{(x-x')^2 + z^2}\mathbf{e}_z \right] \frac{z u(x',t)}{\sqrt{(x-x')^2 + z^2}} dx' \\
&= -\frac{\alpha\kappa}{\beta\pi} v_0 \int_{-L/2}^{L/2} \frac{\mathbf{r} - \mathbf{r}'}{|\mathbf{r} - \mathbf{r}'|^2} \left[\frac{z}{|\mathbf{r} - \mathbf{r}'|} \right] u(x',t) dx', \qquad (4.18)
\end{aligned}$$

where $\mathbf{r} = (x, z)$ and $\mathbf{r}' = (x', 0)$. The main difference from the aster-based velocity distribution considered by Hawkins et al. [15] is the additional factor in square brackets. This is necessary so that the total density $\bar{\rho}(\mathbf{r})$ averaged over all orientations is finite. For simplicity, we will take $L \to \infty$ and $\theta \in [0, \pi]$ in the following. (This is reasonable since $L \gg \xi$.) It follows from (4.17) and (3.16) that

$$\bar{\rho}(\mathbf{r}, t) = \frac{\kappa}{\pi} \int_0^\pi u(x - z\cos\theta/\sin\theta, t) d\theta \qquad (4.19)$$

and

$$Q_{ij}(\mathbf{r}, t) = \frac{\kappa\alpha}{\beta^2} \int_0^\pi u(x - z\mathrm{cotan}(\theta), t) V_i(\theta) V_j(\theta) \frac{d\theta}{\pi}, \qquad (4.20)$$

where $(i, j) \in \{(x, x), (x, z), (z, z)\}$.

4.2.1. Steady-state solution. Let us first calculate the steady-state solution. Equations (3.20) and (4.19) have the x-and t-independent solutions

$$\bar{\rho} = \frac{\kappa u^*}{\pi} \int_0^\pi d\theta = \kappa u^*, \quad u^* = \frac{k_{\mathrm{on}}^*}{k_{\mathrm{off}}} c(0).$$

Substituting these constant solutions into the expressions for Q_{ij} gives

$$\begin{aligned} Q^*_{xx} &= \frac{v_0^2\eta u^*}{\beta}\left[\int_0^\pi \cos^2\theta \frac{d\theta}{\pi}\right] = \frac{v_0^2\eta u^*}{2\beta}, \\ Q^*_{zz} &= \frac{v_0^2\eta u^*}{\beta}\left[\int_0^\pi \sin^2\theta \frac{d\theta}{\pi}\right] = \frac{v_0^2\eta u^*}{2\beta}, \\ Q^*_{xz} &= 0. \end{aligned}$$

Equation (3.14) thus becomes

$$0 = \frac{2v_0\eta u^*}{\pi}\frac{dc}{dz} + D^*_{zz}\frac{d^2c(z)}{dz^2}$$

with $D^*_{zz} = D_0[1-\eta u^*] + Q^*_{zz}$. It follows that

$$c(z) = c(0)\mathrm{e}^{-\xi z}, \quad \xi = 2v_0\eta u^*/\pi D^*_{zz}. \tag{4.21}$$

4.2.2. Stability analysis. Following along lines similar to Case (i), the stability of the steady-state is determined by substituting

$$u(x,t) = u^* + U(k)\mathrm{e}^{ikx+\lambda t}, \quad c(x,z,t) = c(z) + C(k,z)\mathrm{e}^{ikx+\lambda t} \tag{4.22}$$

into (3.14) and (3.20) and Taylor expanding to first order in $U(k)$ and $C(k,z)$. The linear equation corresponding to (3.20) is identical in form to Case (i):

$$(\lambda + D_m k^2 + k_{\mathrm{off}}[1+\eta u^*])U(k) = k^*_{\mathrm{on}}C(k,0). \tag{4.23}$$

The linearized version of (3.14) takes the form

$$\begin{aligned} \lambda C(k,z)\mathrm{e}^{ikx} = &-\frac{\eta}{\pi}\int_0^\pi \mathbf{V}(\theta)\cdot\nabla\left[u^*C(k,z)\mathrm{e}^{ikx} + c(z)\mathrm{e}^{-ikz\mathrm{cotan}(\theta)}U(k)\mathrm{e}^{ikx}\right]d\theta \\ &+\left[D^*_{zz}\frac{d^2C(k,z)}{dz^2} + 2ikD^*_{xz}\frac{dC(k,z)}{dz} - k^2D^*_{xx}C(k,z)\right]\mathrm{e}^{ikx} \\ &+\Delta D_{zz}(k,z)\frac{U(k)}{u^*}\frac{d^2c(z)}{dz^2}\mathrm{e}^{ikx}, \end{aligned} \tag{4.24}$$

where we have canceled common factors of $\mathrm{e}^{\lambda t}$,

$$D^*_{ij} = D_0[1-\eta u^*]\delta_{i,j} + Q^*_{ij}, \tag{4.25}$$

and

$$\Delta D_{zz}(k,z) = -\frac{\kappa\alpha u^*}{\beta}D_0\int_0^\pi \mathrm{e}^{-ikz\mathrm{cotan}(\theta)}\frac{d\theta}{\pi} + \frac{\kappa\alpha u^* v_0^2}{\beta^2}\int_0^\pi \mathrm{e}^{-ikz\mathrm{cotan}(\theta)}\sin^2(\theta)\frac{d\theta}{\pi}. \tag{4.26}$$

Equation (4.24) reduces to the form

$$\begin{aligned} \lambda C(k,z) = &D^*_{zz}\frac{d^2C(k,z)}{dz^2} + \frac{2v_0\eta u^*}{\pi}\frac{dC(k,z)}{dz} - k^2D^*_{xx}C(k,z) \\ &+\eta U(k)\left(v_0\frac{dc}{dz}g_s(kz) + \left[\frac{v_0^2}{\beta}f_s(kz) - D_0 f(kz)\right]\frac{d^2c(z)}{dz^2}\right), \end{aligned} \tag{4.27}$$

where (see the appendix)

$$f(q) \equiv \int_0^\pi \mathrm{e}^{-iq\cot an(\theta)} \frac{d\theta}{\pi} = \mathrm{e}^{-|q|}, \tag{4.28a}$$

$$g_s(q) \equiv \int_0^\pi \mathrm{e}^{-iq\cot an(\theta)} \sin\theta \frac{d\theta}{\pi} = \frac{2}{\pi}|q|K_1(|q|), \tag{4.28b}$$

$$f_s(q) \equiv \int_0^\pi \mathrm{e}^{-iq\cot an(\theta)} \sin^2\theta \frac{d\theta}{\pi} = \frac{1+|q|}{2} f(q) \tag{4.28c}$$

with K_1 a modified Bessel function of order $n = 1$.

Equation (4.27) can be rewritten as the linear, inhomogeneous equation

$$\widehat{L}_z C(k,z) = -h(k,z)C(k,0), \tag{4.29}$$

with $C(k,\infty) = 0$,

$$\widehat{L}_z C \equiv D^*_{zz}\frac{d^2C}{dz^2} + \frac{2v_0\eta u^*}{\pi}\frac{dC}{dz} - [\lambda + k^2 D^*_{xx}]C \tag{4.30}$$

and

$$h(k,z) \equiv \Theta(k)\mathrm{e}^{-\xi z}\left[C_1 g_s(kz) + C_2 f_s(kz) + C_3 f(kz)\right]. \tag{4.31}$$

Note that we have substituted for $U(k)$ using (4.23), written in the form

$$\frac{U(k)}{C(k,0)}\frac{c(0)}{u^*} = \Theta(k), \quad \Theta(k) \equiv \frac{k_{\mathrm{off}}}{\lambda + D_m k^2 + k_{\mathrm{off}}[1+\eta u^*]}, \tag{4.32}$$

and set

$$C_1 = -\eta u^* v_0 \xi, \quad C_2 = \frac{\eta u^* \xi^2 v_0^2}{\beta}, \quad C_3 = -\eta u^* \xi^2 D_0. \tag{4.33}$$

Equation (4.29) can be solved using Green's functions. That is, let $G(z,z')$ satisfy the equation

$$\widehat{L}_z G(z,z') = \delta(z-z'), \quad G(0,z') = 0, \quad G(\infty,z') = 0. \tag{4.34}$$

A standard calculation yields

$$G(z,z') = \begin{cases} \dfrac{e^{-\rho_1 z + \rho_2 z'} - \mathrm{e}^{-\rho_2(z-z')}}{D^*_{zz}(\rho_1 - \rho_2)} & \text{if } z < z', \\[2ex] \dfrac{\mathrm{e}^{-\rho_1 z + \rho_2 z'} - \mathrm{e}^{-\rho_1(z-z')}}{D^*_{zz}(\rho_1 - \rho_2)} & \text{if } z > z', \end{cases} \tag{4.35}$$

where

$$\rho_1 = \frac{v_0\eta u^*/\pi + \sqrt{(v_0\eta u^*/\pi)^2 + D^*_{zz}[\lambda + D^*_{xx}k^2]}}{D^*_{zz}} > 0,$$

$$\rho_2 = \frac{v_0\eta u^*/\pi - \sqrt{(v_0\eta u^*/\pi)^2 + D^*_{zz}[\lambda + D^*_{xx}k^2]}}{D^*_{zz}} < 0.$$

Taking into account the boundary conditions, we find that the solution to (4.29) is

$$\frac{C(k,z)}{C(k,0)} = -\int_0^\infty G(z,z')h(k,z')dz' + \mathrm{e}^{-\rho_1 z}. \tag{4.36}$$

4.2.3. Dispersion relation. The final step is to derive the dispersion equation $\lambda = \lambda(k)$ by considering the linearized version of the flux conservation equation (3.17):

$$D^*_{zz}\frac{\partial C(k,z)}{\partial z}\Big|_{z=0} - \xi\Delta D_{zz}(k,0)c(0)\frac{U(k)}{u^*} + \frac{2\eta v_0}{\pi}[u^*C(k,0)+c(0)U(k)] = k^*_{\rm on}C(k,0) - k_{\rm off}(1+\eta u^*)U(k), \tag{4.37}$$

where ΔD_{zz} is given by (4.26) for $z=0$,

$$\Delta D_{zz}(k,0) = -\eta u^* D_0 + \frac{\eta u^* v_0^2}{2\beta},$$

which is independent of k. Substituting for $C(k,z)$ using (4.36) and noting that $D^*_{zz}\partial_z G(z,z')|_{z=0} = -{\rm e}^{\rho_2 z'}$, we have

$$\frac{D^*_{zz}}{C(k,0)}\frac{\partial C(k,z)}{\partial z}\Big|_{z=0} = -D^*_{zz}\rho_1 + \Theta(k)\int_0^\infty {\rm e}^{-[\xi-\rho_2]z'}\left[C_1 g_s(kz') + C_2 f_s(kz') + C_3 f(kz')\right]dz'. \tag{4.38}$$

We can evaluate the integrals involving the functions $f(kz)$ and $f_s(kz)$ explicitly:

$$\begin{aligned}\int_0^\infty {\rm e}^{-\rho_1 z} f_s(kz)dz &= \frac{1}{2}\int_0^\infty {\rm e}^{-(\rho_1+k)z}(1+kz)dz \\ &= \frac{1}{2(\rho_1+k)} + \frac{k}{2(\rho_1+k)^2} = \frac{2k+\rho_1}{2(k+\rho_1)^2},\\ \int_0^\infty {\rm e}^{-\rho_1 z} f(kz)dz &= \int_0^\infty {\rm e}^{-(\rho_1+k)z}dz = \frac{1}{k+\rho_1},\end{aligned}$$

where we have used the identity $\rho_1+\rho_2 = 2v_0\eta u^*/(\pi D^*_{zz}) = \xi$. In the case of $g_s(kz)$, $k\neq 0$, we have

$$\begin{aligned}G_s(k,\rho_1) \equiv \int_0^\infty e^{-\rho_1 z} g_s(kz)dz &= \frac{1}{k}\int_0^\infty e^{-\rho_1 z'/k} g_s(z')dz' \\ &= \frac{2}{k\pi}\int_0^\infty e^{-\rho_1 z'/k} z' K_1(z')dz' \\ &= \frac{2}{k\pi}\left[\frac{\rho_1/k}{(\rho_1/k)^2-1} - \frac{\operatorname{arccosh}(\rho_1/k)}{(\rho_1^2/k^2-1)^{3/2}}\right].\end{aligned}$$

On the other hand, if $k=0$, then

$$G_s(0,\rho_1) = \int_0^\infty e^{-\rho_1 z} g_s(0)dz = \frac{2}{\pi}\int_0^\infty e^{-\rho_1 z}dz = \frac{2}{\pi\rho_1}.$$

Finally, combining (4.37) and (4.38) and (4.32), we can eliminate a common factor of $C(k,0)$ to obtain the equation

$$(D^*_{zz}[\xi-\rho_1] - k^*_{\rm on}) + \Theta(k)\int_0^\infty {\rm e}^{-\rho_1 z'}\left[C_1 g_s(kz') + C_2 f_s(kz') + C_3 f(kz')\right]dz' = \left[\xi\Delta D_{zz}(k,0) - D^*_{zz}\xi - (1+\eta u^*)k^*_{\rm on}\right]\Theta(k).$$

Substituting for $\Theta(k)$, this reduces to (see also (4.14))

$$
\begin{aligned}
0 = {} & [\xi \Delta D_{zz}(k,0) - D^*_{zz}\xi - D^*_{zz}(\xi-\rho_1)(1+\eta u^*)]\,\frac{k_{\rm off}}{D^*_{zz}} \\
& + \left[\frac{k^*_{\rm on}}{D^*_{zz}} - (\xi-\rho_1)\right]\left[\lambda + D_m k^2\right] \\
& - \frac{k_{\rm off}}{D^*_{zz}}\int_0^\infty \mathrm{e}^{-\rho_1 z'}\left[C_1 g_s(kz') + C_2 f_s(kz') + C_3 f(kz')\right] dz'.
\end{aligned} \tag{4.39}
$$

5. Numerical results and discussion. Example dispersion curves $\lambda = \lambda(k)$ for the nucleation configuration (Case (ii)) are plotted in Figure 8(a). Consistent with the results of Hawkins et al. [15], we find that there is a finite range of wave numbers $(0, k_c]$ for which $\lambda(k) > 0$, with a maximum at $k = k_{max}$. This maximum corresponds to a dominant (fastest growing) instability of finite characteristic length $2\pi/k_{\rm max}$. We also see that $k_{\rm max}$ increases with ξ, as illustrated in Figure 8(b). For ease of presentation, we treat k as a continuous variable, which holds when $L \to \infty$. For finite L and periodic boundary conditions with respect to x, the dispersion curves are discretely sampled at the points $k = 2\pi m/L$ for integer m. Given a particular cell circumference $L = 2\pi R$, cell polarization patches will be observed if $2\pi/k_{\rm max} < L$, that is, $k_{\rm max}R > 1$. Indeed, as ξ increases, $k_{\rm max}$ crosses a sequence of thresholds given by $k_{\rm max}R = n_c$ for positive integers n_c, such that n_c patches form. The occurrence of the most common polarization pattern ($n_c = 1$) is illustrated in Figure 8(b).

One major feature of our model is that there are additional biophysical parameters such as the motor speed v_0 and unbinding rate β, both of which affect the dispersion curves and the value of k_{max}; see Figure 9. In Figure 10, we show plots of the wavenumber $k_{\rm max}$ and inverse growth rate $\tau = \lambda(k_{\rm max})^{-1}$ of the fastest growing eigenmode as functions of v_0 and β. It can be seen, for example, that $k_{\rm max}$ is a decreasing function of v_0 and an increasing function of β. Hence, our model identifies parameters associated with motor transport that can be tuned to generate spontaneous cell polarization, beyond the total number of molecules M and the coupling

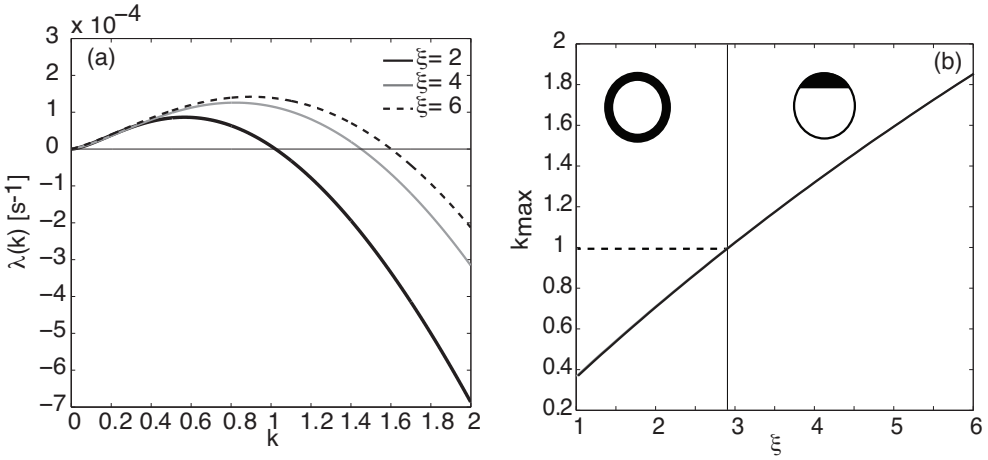

FIG. 8. (a) *Dispersion curves for nucleation model for various ξ. Same parameter values as Figure* 6. (b) *Variation of $k_{\rm max}$ with ξ. Same parameter values as* (a) *except $v_0 = 0.1\,\mu m s^{-1}$, $\bar{k}_{\rm on} = 0.5\,\mu m s^{-1}$. Both ξ and k are in units of R^{-1}.*

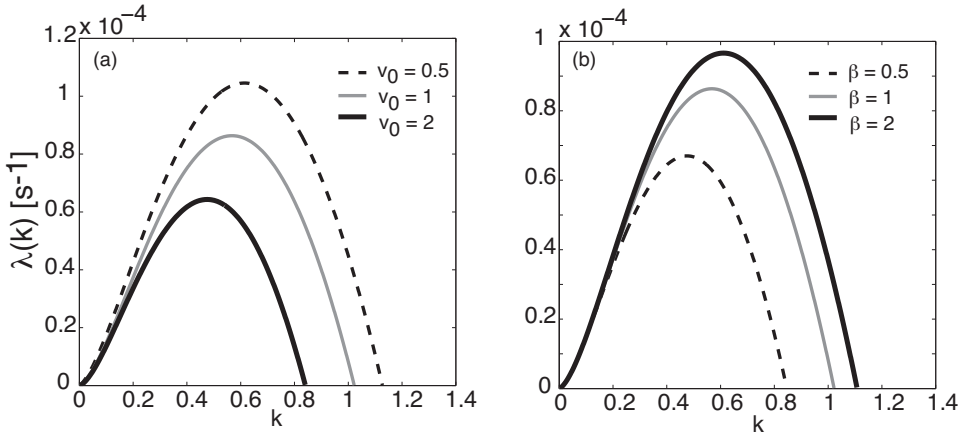

FIG. 9. *Dispersion curves for different values of* (a) *speed* v_0 *with* $\beta = 1s^{-1}$ *and* (b) *unbinding rate* β *with* $v_0 = 1\,\mu m s^{-1}$. *Other parameters:* $D_0 = 0.1\,\mu m^2\,s^{-1}$, $D_m = 0.01\,\mu m^2\,s^{-1}$, $R = 10\,\mu m$, $k_{\rm off} = 0.1s^{-1}$, $\bar{k}_{on} = 1\,\mu m s^{-1}$, $\xi = 2$. *Both* ξ *and* k *are in units of* R^{-1}.

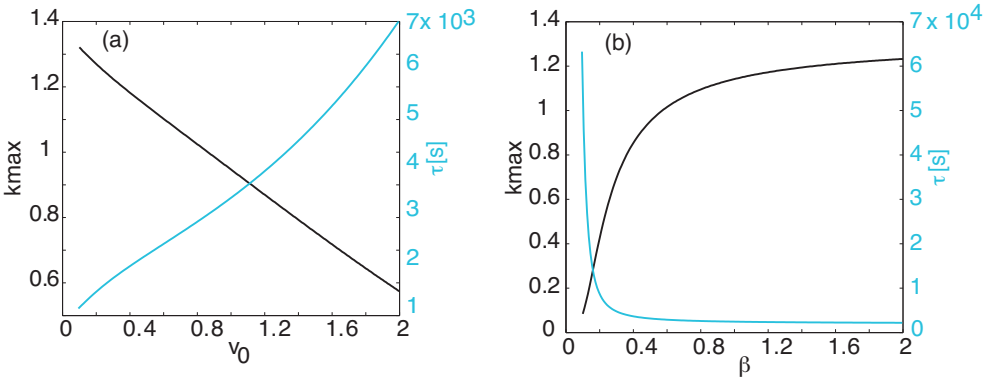

FIG. 10. *Plots of wavenumber* $k_{\max}$ *and inverse growth rate* $\tau = \lambda(k_{\max})^{-1}$ *for the faster growing eigenmode as a function of* (a) *motor speed* v_0 *and* (b) *unbinding rate* β. *Baseline parameters are* $\beta = 1\,s^{-1}$, $\xi = 4, v_0 = 0.5\,\mu m s^{-1}, \bar{k}_{\rm on} = 0.5\,\mu m s^{-1}$. *Other parameters are the same as in Figure* 6.

parameter κ. Finally, note that it is not possible to reduce our model to Case (ii) of [15], since we take a different expression for the aster velocity field (see (4.18)), which is necessary in order to generate the velocity field from a normalizable distribution of filaments. Nevertheless, one can obtain a good match between the two models by slightly changing the baseline parameters in our model. This is illustrated in Figures 11 and 12.

In conclusion, the effects of cytoskeletal geometry on cell polarization identified in [15] persist when biophysical details regarding motor-driven vesicular transport are taken into account. One outstanding challenge is to understand how the vesicular transport of signaling proteins such as Cdc42 [9] can enhance the membrane-bound concentration of the proteins. This will require a more detailed model of the fusion and budding of vesicles with the cell membrane. Another extension of our model is to consider cell polarization driven by external stimuli. This then raises two interesting

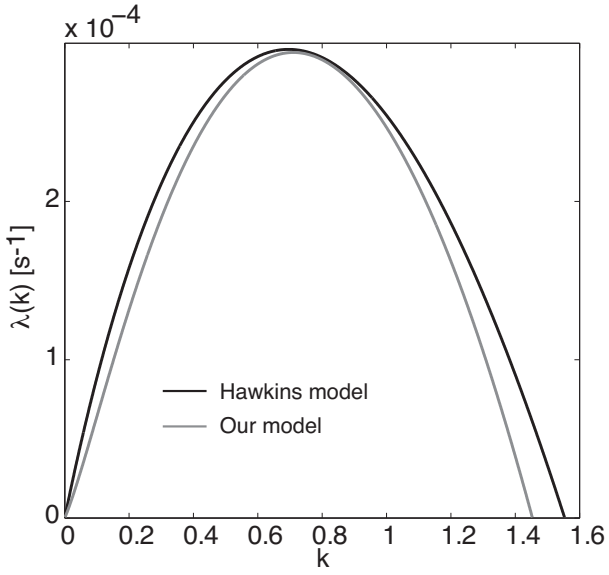

FIG. 11. *Comparison of dispersion curves generated from our model and the model of Hawkins et al. Parameters of our model:* $\beta = 1\,s^{-1}, \xi = 2, v_0 = 0.1\,\mu m s^{-1}, \bar{k}_{\rm on} = 0.5\,\mu m s^{-1}$. *Other parameters are the same as in Figure* 6.

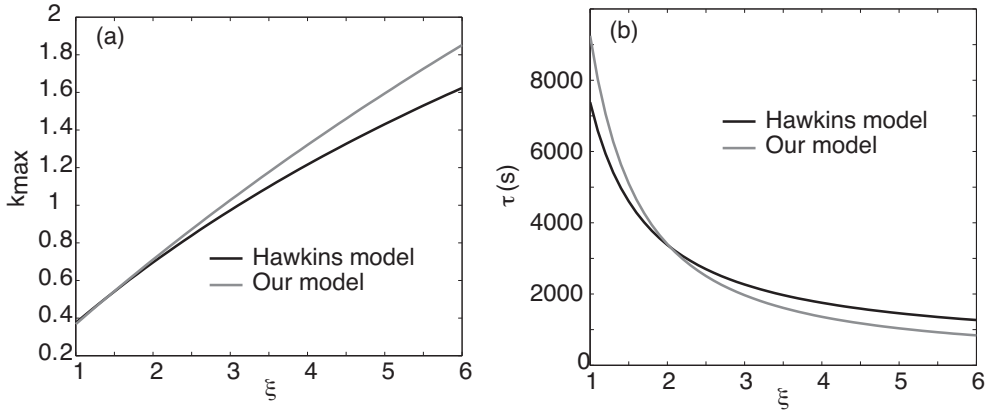

FIG. 12. *Plots of* (a) *wavenumber* $k_{\rm max}$ *and* (b) *inverse growth rate* $\tau = \lambda(k_{\rm max})^{-1}$ *for the faster growing eigenmode as a function of* ξ. *Parameters of our model:* $\beta = 1s^{-1}, \xi = 2, v_0 = 0.1\,\mu m s^{-1}, \bar{k}_{\rm on} = 0.5\,\mu m s^{-1}$. *Other parameters are the same as in Figure* 6. *Corresponding plots of the Hawkins et al. model are shown for comparison.*

questions: Can our model account for driven polarization? How sensitive is the response? As proposed in Hawkins et al. [15], one can assume there is an activator gradient which results in an asymmetric activation of the signaling molecules on the membrane. One way to implement this is to assume a spatial inhomogeneity in the parameter constant κ, the proportionality constant between the density ρ of actin filaments and the concentration of membrane-bound molecules $u(x,t)$. Finally, in our stability analysis we assumed that the density of filaments was sufficiently small so that we could carry out a perturbation expansion with respect to $a(\mathbf{r})$; see (3.13).

In order to determine the accuracy of such an approximation, it would be necessary to develop a more detailed model of a cytoplasmic motor-cargo complex interacting with a discrete network of cytoskeletal filaments. One could then use homogenization theory to calculate an effective space-dependent binding rate, as well as determining the effects of molecular crowding on the diffusivity of vesicles in the cytoplasm.

Appendix. The integrals $f(q)$, $f_s(q)$, and $g_s(q)$ can be evaluated as follows:

$$f(q)=\int_0^\pi \mathrm{e}^{-iq\mathrm{cotan}(\theta)}\frac{d\theta}{\pi}=\frac{1}{\pi}\int_{-\infty}^{\infty}\mathrm{e}^{-iqr}\frac{dr}{1+r^2}=\mathrm{e}^{-|q|} \tag{A.1}$$

and

$$\begin{aligned} f_s(q)&\equiv\int_0^\pi \mathrm{e}^{-iq\mathrm{cotan}(\theta)}\sin^2\theta\frac{d\theta}{\pi}=\frac{1}{\pi}\int_{-\infty}^{\infty}\mathrm{e}^{-iqr}\frac{1}{1+r^2}\frac{dr}{1+r^2}\\ &=-\frac{1}{2a}\frac{d}{da}\frac{1}{\pi}\int_{-\infty}^{\infty}\mathrm{e}^{-iqr}\frac{dr}{a^2+r^2}\Big|_{a=1}=-\frac{1}{2a}\frac{d}{da}\frac{e^{-a|q|}}{a}\Big|_{a=1}\\ &=\left(\frac{1}{2a}\frac{e^{-a|q|}}{a^2}+\frac{|q|}{2a}\frac{e^{-a|q|}}{a}\right)_{a=1}=\frac{1+|q|}{2}f(q). \end{aligned} \tag{A.2}$$

Similarly,

$$\begin{aligned} g_s(q)&=\int_0^\pi \mathrm{e}^{-iq\mathrm{cotan}(\theta)}\sin\theta\frac{d\theta}{\pi}=\frac{1}{\pi}\int_{-\infty}^{\infty}\mathrm{e}^{-iqr}\frac{1}{\sqrt{1+r^2}}\frac{dr}{1+r^2}\\ &=\frac{1}{\pi}\int_{-\infty}^{\infty}\frac{\cos(qr)}{\sqrt{1+r^2}}\frac{dr}{1+r^2}=\frac{2}{\pi}\int_0^{\infty}\frac{\cos(qr)}{\sqrt{1+r^2}}\frac{dr}{1+r^2}\\ &=-\frac{1}{a}\frac{d}{da}\frac{2}{\pi}\int_0^{\infty}\frac{\cos(qr)}{\sqrt{a^2+r^2}}dr\Big|_{a=1}. \end{aligned}$$

Noting that the modified Bessel function of the second kind of order $n=0$ has the integral representation $K_0(q)=\int_0^\infty \frac{\cos(qr)}{\sqrt{1+r^2}}dr$, we have

$$g_s(q)\ =-\frac{1}{a}\frac{d}{da}\left[\frac{2}{\pi}K_0(aq)\right]\Big|_{a=1}=-\frac{2}{\pi}|q|K_0'(|q|)=\frac{2}{\pi}|q|K_1(|q|). \tag{A.3}$$

where $K_1(x)$ is the modified Bessel function of the second kind of order $n=1$. In particular, $g_s(0)=2/\pi$.

REFERENCES

[1] S. J. Altschuler, S. B. Angenent, Y. Wang, and L. F. Wu, *On the spontaneous emergence of cell polarity*, Nature, 454 (2008) pp. 886–890.

[2] N. Arimura and K. Kaibuchi, *Neuronal polarity: From extracellular signals to intracellular mechanisms,* Nat. Rev. Neurosci. 8 (2007), pp. 194–205.

[3] O. Benichou, C. Loverdo, M. Moreau, and R. Voituriez, *A minimal model of intermittent search in dimension two,* J. Phys. A, 19 (2007), 065141.

[4] C. Bouzigues, M. Morel, A. Triller, and M. Dahan, *Asymmetric redistribution of GABA receptors during GABA gradient sensing by nerve growth cones analyzed by single quantum dot imaging,* Proc. Natl. Acad. Sci. USA, 104 (2007), pp. 11251–11256.

[5] P. C. Bressloff and J. M. Newby, *Quasi-steady state analysis of motor-driven transport on a two-dimensional microtubular network,* Phys. Rev. E, 83 (2011), 061139.

[6] P. C. Bressloff and J. M. Newby, *Stochastic models of intracellular transport,* Rev. Mod. Phys, 85 (2013), pp. 135–196.

[7] P. C. Bressloff and J. M. Newby, *Metastability in a stochastic neural network modeled as a jump velocity Markov process,* SIAM J. Appl. Dyn. Syst., 12 (2013), pp. 1394–1435.
[8] P. C. Bressloff, *Stochastic Processes in Cell Biology,* Springer, New York, 2014.
[9] S. A. Dighe and K. G. Kozminski, *Secretory vesicles deliver Cdc42p to sites of polarized growth in* S. cerevisiae, PLoS One, 9 (2014), e99494.
[10] A. Friedman and G. Craciun, *A model of intracellular transport of particles in an axon,* J. Math. Biol., 51 (2005), pp. 217–246.
[11] A. Friedman and G. Craciun, *Approximate traveling waves in linear reaction-hyperbolic equations,* SIAM J. Math. Anal., 38 (2006), pp. 741–758.
[12] A. Gamba, I. Kolokolov, V. Lebedev, and G. Ortenzi, *Universal features of cell polarization processes,* J. Stat. Mech. (2009), P02019.
[13] C. W. Gardiner, *Handbook of Stochastic Methods,* 4th ed. Springer, Berlin, 2009.
[14] A. B. Goryachev and A. V. Pokhilko, *Dynamics of Cdc42 network embodies a Turing-type mechanism of yeast cell polarity,* FEBS Lett., 582 (2008), pp. 1437–1443.
[15] R. J. Hawkins, O. Benichou, M. Piel, and R. Voituriez, *Rebuilding cytoskeleton roads: active-transport-induced polarization of cell,* Phys. Rev. E, 80 (2009), 040903(R).
[16] T. Hillen and H. Othmer, *The diffusion limit of transport equations derived from velocity-jump processes,* SIAM J. Appl. Math., 61 (2000), pp. 751–775.
[17] A. S. Howell, N. S. Savage, S. A. Johnson, I. Bose, A. W. Wagner, T. R. Zyla, H. F. Nijhout, M. C. Reed, A. B. Goryachev, and D. J. Lew, *Singularity in polarization: Rewiring yeast cells to make two buds,* Cell, 139 (2009), pp. 731–743.
[18] A. Jilkine and L. Edelstein-Keshet, *A comparison of mathematical models for polarization of single eukaryotic cells in response to guided cues,* PLoS Comput. Biol., 7 (2011), e1001121.
[19] A. Jilkine, S. B. Angenent, L. F. Wu, and S. J. Altschuler, *A density-dependent switch drives stochastic clustering and polarization of signaling molecules,* PLoS Comput. Biol., 7 (2011), e1002271.
[20] J. M. Johnson, M. Jin, and D. J. Lew, *Symmetry breaking and the establishment of cell polarity in budding yeast,* Curr. Opin. Gen. Dev., 21 (2011), pp. 740–746.
[21] F. Julicher, A. Ajdari, and J. Prost, *Modeling molecular motors*, Rev. Mod. Phys., 69 (1997), pp. 1269–1281.
[22] D. Keller and C. Bustamante, *The mechanochemistry of molecular motors,* Biophys. J., 78 (2000), pp. 541–556.
[23] A. Kolomeisky and M. Fisher, *Molecular motors: A theorist's perspective,* Ann. Rev. Phys. Chem., 58 (2007), 675–695.
[24] M. J. Lawson, B. Drawert, M. Khammash, L. Petzoldand, and T.-M. Yi, *Spatial stochastic dynamics enable robust cell polarization,* PLoS Comput. Biol., 9 (2012), e1003139.
[25] A. T. Layton, N. S. Savage, A. S. Howell, S. Y. Carroll, D. G. Drubin, and D. J. Lew, *Modeling vesicle traffic reveals unexpected consequences for Cdc42p-mediated polarity establishment,* Curr. Biol., 21 (2011), pp. 184–194.
[26] R. Lipowsky and S. Klumpp, *'Life is motion': multiscale motility of molecular motors,* Phys. A, 352 (2005), pp. 53–112.
[27] E. Marco, R. Wedlich-Soldner, R. Li, S. J. Altschuler, and L. F. Wu, *Endocytosis optimizes the dynamic localization of membrane proteins that regulate cortical polarity,* Cell, 129 (2007), pp. 411–422.
[28] A. J. McKane, T. Biancalani, and T. Rogers, *Stochastic pattern formation and spontaneous polarization: The linear noise approximation and beyond*, Bull. Math. Biol., 76 (2014), pp. 895–921.
[29] S. A. Menchon, A. Gartner, P. Roman, and C. G. Dotti, *Neuronal (bipolarity) as a self-organized process enhanced by growing membrane,* PLoS One, 6 (2011), e24190.
[30] Y. Mori, A. Jilkine, and L. Edelstein-Keshet, *Wave-pinning and cell polarity from a bistable reaction-diffusion system,* Biophys. J., 94 (2008), pp.3684–3697.
[31] D. Neukirchen and F. Bradke, *Neuronal polarization and the cytoskeleton,* Sem. Cell Dev. Biol., 22 (2011), pp. 825–833.
[32] J. M. Newby and P. C. Bressloff, *Quasi-steady state reduction of molecular-based models of directed intermittent search,* Bull. Math. Biol., 72 (2010), pp. 1840–1866.
[33] J. M. Newby and P. C. Bressloff, *Local synaptic signaling enhances the stochastic transport of motor-driven cargo in neurons,* Phys., Biol., 7 (2010), 036004.
[34] H. Othmer, S. Dunbar, and W. Alt, *Models of dispersal in biological systems,* J. Math. Biol., 26 (1988), pp. 263–298.

[35] G. C. Papanicolaou, *Asymptotic analysis of transport processes,* Bull. Amer. Math. Soc., 81 (1975), pp. 330–392.
[36] M. C. Reed, S. Venakides, and J. J. Blum, *Approximate traveling waves in linear reaction-hyperbolic equations,* SIAM J. Appl. Math., 50 (1990), pp. 167–180.
[37] N. S. Savage, A. T. Layton, and D. J. Lew, *Mechanistic model of polarity in yeast,* Mol. Biol. Cell, 23 (2012), pp. 1998–2013.
[38] M. Semplice, A. Veglio, G. Naldi, G. Serini, and A. Gamba, *A bistable model of cell polarity,* PLoS One, 7 (2012), e30977.
[39] B. D. Slaughter, S. E. Smith, and R. Li, *Symmetry breaking in the life cycle of budding yeast,* Cold Spring Harb. Perspect. Biol., 1 (2009), a003384.
[40] B. D. Slaughter, A. Das, J. W. Schwartz, B. Rubinstein, and R. Li, *Dual modes of Cdc*42 *recycling fine-tune polarized morphogenesis,* Dev. Cell, 17 (2009), pp. 823–835.
[41] T. Tojima, *Intracellular signaling and membrane trafficking control bidirectional growth cone guidance,* Neurosci. Res., 73 (2012), pp. 260–274.
[42] R. Wedlich-Soldner, S. C. Wai, T. Schmidt, and R. Li, *Robust cell polarity is a dynamic state established by coupling transport and GTPase signaling,* J. Cell. Biol., 166 (2004), pp. 889–900.